

Received 4 October 2023, accepted 8 November 2023, date of publication 13 November 2023, date of current version 16 November 2023.

Digital Object Identifier 10.1109/ACCESS.2023.3332203

RESEARCH ARTICLE

A Reactive Voltage Compensation-Based Control Scheme to Extend Speed Range in Five Phase Open-End Winding Induction Motor Drives

PRASOON CHANDRAN MAVILA¹, (Member, IEEE),

AND P. P. RAJEEVAN¹, (Senior Member, IEEE)

Department of Avionics, Indian Institute of Space Science and Technology, Thiruvananthapuram 695547, India

Corresponding author: P. P. Rajeevan (rajeevanpp@iist.ac.in)

ABSTRACT A reactive voltage compensation based control scheme for extending the speed range in dual inverter-fed five phase induction motor drives with open-end stator windings is proposed in this paper. In the dual inverter-fed five phase drive topology used to implement the proposed control scheme, one inverter is powered from a DC source while a charged capacitor acts as the DC-link of the other inverter. Since the control scheme is developed by considering the motor current vector as the reference, the motor voltage can be resolved into its active and reactive components. The capacitor-fed inverter is controlled in such a way that it compensates the increasing reactive voltage drop inside the motor as the speed increases, thereby extending the constant power speed region of the drive. The scheme also ensures that the voltage across the capacitor is maintained at the required level, under all operating conditions of the drive. This feature also safeguards the capacitor against overcharging. In addition, the auxiliary plane harmonics generated by both inverters are nullified in an average sense, in a switching period. The proposed control scheme is substantially simpler compared to the existing schemes, due to the unified PWM scheme and reduction in PI controllers. The experimental validation of the proposed scheme is carried out on an open-end winding induction motor under transient as well as steady state operating conditions. TMS320F28335 DSP based digital controller is used for implementation of the control algorithm.

INDEX TERMS Five phase induction motor, open-end winding, speed range extension.

I. INTRODUCTION

In recent years, there has been an increase in research interest in multiphase motor drives centering around many high power and safety critical applications. This is attributed to their inherent benefits, such as reduced voltage and current ratings per phase for a given power rating, higher fault tolerance, higher power density, and lower torque ripple compared to three phase motor drives [1], [2], [3], [4], [5]. Induction motors, considered to be the work horse of the industry, are often a choice for many such applications like the spindle drives and electric vehicles (EVs) where the drives are required to operate over a wide speed range with the

maximum speed reaching far above the base speed [3], [4], [5]. As the speed of the induction motor increases, the back EMF increases proportionally if the flux is maintained constant. In addition to this, the reactive voltage drop across the motor inductance also increases with increase in frequency, as the speed increases. Thus, the increase in the voltage requirement and the reactive power requirement of the motor must be met to extend the operating speed range of the motor. But the capability of the inverter to produce adequate voltage to overcome the back EMF is constrained by the DC-link voltage available. One common method to increase the operating speed beyond the base speed is by adopting field weakening so that the back EMF can be maintained constant [6], [7] even when the speed is increasing. In this region of operation, known as constant power speed range,

The associate editor coordinating the review of this manuscript and approving it for publication was Feifei Bu¹.

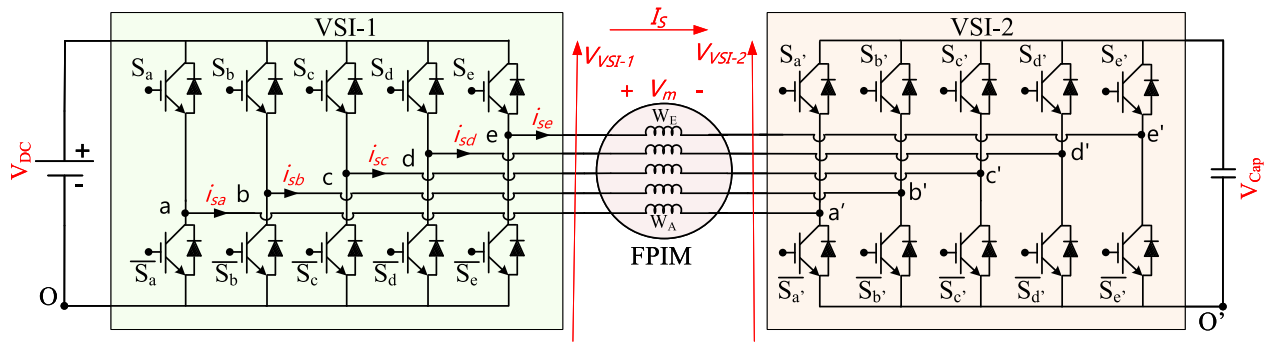


FIGURE 1. Circuit schematic of dual inverter-fed five phase induction motor with open-end stator windings, with VSI-1 fed from a DC source and VSI-2 fed from a charged capacitor.

the torque is reduced with increase in speed so as to keep the output power of the machine at its rated value. However, the maximum speed attainable in this region is constrained by the significant increase in the reactive voltage drop across the motor inductance at high speeds.

A possible approach to overcome this limitation is that either the DC source voltage must be high enough to support the extended speed range of operation, or the converter configuration must be able to provide enhanced output voltage from a given battery voltage, to compensate for the increased reactive voltage drop.

The dual inverter configuration where the open-ended stator windings of the induction motor are supplied from two voltage source inverters (VSIs) is a popular choice for the output voltage enhancement. In addition to the enhanced voltage output, the dual inverter configuration provides benefits such as power-sharing between the inverters, reduced dv/dt , higher reliability and multilevel output voltage waveform, making it a suitable candidate for many medium and high power applications. The conventional dual inverter configuration uses two isolated DC sources (often batteries) to supply the individual VSIs. The isolated DC sources inherently eliminate the flow of zero sequence circulating currents. However, the isolated DC sources in turn can increase the size and cost of the system, and these limitations could make it unsuitable for certain applications such as electric vehicles (EV).

Alternatively, a single DC source can be used to supply the VSIs using a common DC-link, if the zero sequence circulating currents can be eliminated. However, this restricts the use of all possible switching states, resulting in reduced output voltage and the loss of multilevel output voltage profile compared to the configuration with isolated DC sources. Another configuration is to have a charged capacitor to replace the DC source of one of the VSIs, if no active power needs to be delivered by this VSI (Fig. 1). Since there is no common DC-link, this configuration naturally eliminates zero-sequence circulating current. This drive configuration has the capability to extend the speed range as reported in the literature for three phase drives [8], [9], [10], [11].

However, very few such schemes have been reported in the literature so far, for the control of five phase induction

motor drives [12], [13]. The application of such schemes to multiphase drives is quite complex and not straight forward as it requires a different approach to deal with the voltages in multiple two-dimensional space vector planes existing in the multi-phase systems, in contrast to a single fundamental ($\alpha\beta$) space vector plane in a 3-phase drive. For example, each of the switching state in a five phase VSI maps to two space vector planes, known as fundamental ($\alpha\beta$ -plane), and auxiliary (xy -plane) planes. Any voltage generated in the xy -plane represents the existence of low order voltage harmonics of order 3, 7, 13 etc., even when pulse width modulation (PWM) strategies are adopted. These harmonics do not contribute to the torque production in a five phase induction motor (FPIM) with distributed stator windings. Their presence, unopposed by back EMF, leads to large harmonic currents that are limited only by stator resistance and leakage impedance of the motor. This leads to increase in losses in the system along with underutilization of stator core for useful flux [1], [16]. Therefore, the control schemes in a FPIM drive must take care of the elimination of these xy -plane voltage harmonics along with the control of voltage in the fundamental plane.

In order to have clear idea about the novelty of the proposed control scheme it has to be compared with the existing control schemes for five phase induction motor drives with open end stator windings in which a DC source fed inverter is connected to one side of the windings and a capacitor fed inverter is connected to the other side of the windings. The control scheme presented in [12] used a variable capacitor voltage fed VSI based speed control scheme for a dual inverter fed FPIM drive, focused on the optimization of the DC voltage. The scheme used two dedicated PI controllers for the control of the capacitor fed VSI. One of these controllers was allocated for capacitor voltage regulation and the other was used for power factor correction, similar to that presented in [8] for a 3-phase drive.

Nevertheless, the issue associated with the generation of 3rd harmonic voltage was dealt in [12] using two additional inner current control loops, resulting in two extra PI controllers. The performance of these PI controllers was affected by the DC-link voltage ripple [12], [13]. Moreover, the scheme used a variable capacitor voltage, and the modulation

index of floating bridge was maintained between a band of 0.85 to 0.95 using hysteresis control method, to prevent the overcharging and voltage overshoot of the capacitor. It has been established that the voltage fluctuations could negatively impact the life of the capacitor [14]. Besides, there are seven PI controllers in the scheme presented in [12] making the control scheme very complex to implement since the tuning of these seven PI controllers is extremely difficult and very laborious. The scheme in [12] was further explored in [13], in which a generalized control approach was presented for multiphase drives, incorporating the compensation scheme for unbalance in the stator current reported in [15]. The number of control loops and PI controllers required could be more than seven for a five phase system for the scheme presented in [13], depending on the number of harmonic voltages to be suppressed (excluding the additional controllers required if stator current unbalance needs to be compensated).

Nonetheless, the schemes reported in [12] and [13] have not explored the charged capacitor-fed dual inverter configuration for the specific application of extending the constant power speed range of multiphase drives. On the other hand, the focus of the proposed control scheme is to extend the constant power speed range of dual inverter-fed five phase open-end winding induction motor drives. The proposed scheme presents a greatly simplified control approach compared to that in [12] and [13] without compromising the performance, as explained in the following paragraphs.

The major differences of the scheme proposed in this paper compared to the schemes reported in [12] and [13] are as follows.

- The proposed scheme is much simpler compared to the schemes reported in [12] and [13] mainly due to the substantial reduction in the number of PI controllers required. The schemes presented in [12] and [13] require a minimum of seven PI controllers whereas the proposed scheme requires only two PI controllers if constant V/f ratio control is employed and four PI controllers when vector control is employed for the motor control.
- The DC source fed VSI operate with unity power factor (UPF) in the entire operating range without any dedicated controller for the same.
- In the proposed scheme the suppression of harmonic voltages in xy-plane, like 3rd, 7th and 13th harmonics, are carried out using a voltage space vector based switching scheme without using any PI controllers. In contrast, the schemes in [12] and [13] use dedicated PI controllers for suppressing only the 3rd harmonic current. For suppressing other auxiliary plane harmonic currents like the 7th and 13th harmonics, additional PI controllers are required. As stated in [12] and [13], it is extremely difficult to tune these PI controllers due to the very low impedance offered by the motor to the auxiliary plane harmonic currents. In contrast, the elimination of xy-plane voltage harmonics in the proposed scheme is not dependent on the impedance of the stator or gain of

the controller since it is based on a voltage space vector based switching scheme.

- In the proposed scheme the capacitor voltage is decided based on the maximum reactive power requirement of the drive and it is held constant under all operating conditions of the drive. This feature prevents damages due to overcharging of the capacitor or voltage overshoot during dynamic operating conditions.
- The proposed scheme enables the charging of the capacitor, and the reactive power compensation during the start-up process itself and does not require pre-charging of the capacitor. On the other hand, in the schemes reported in [12] and [13], the capacitor has to be pre-charged before the start-up of the motor, and reactive power compensation is enabled only when the drive reaches steady state, to avoid overshoot of capacitor voltage.

This article is organized as follows: The basic power circuit configuration is described in section II. The voltage space vector decomposition used in the proposed scheme for the elimination of xy-plane voltage harmonics detailed in Section III. The decoupling of active and reactive power requirement of the drive for speed range extension, and control scheme for the two inverters are elaborated in Section IV. Experimental results and conclusions are given in section V and section VI, respectively.

II. POWER CIRCUIT CONFIGURATION

The circuit schematic of the dual inverter fed five phase induction motor with open-end stator windings used in the proposed speed range extension scheme is shown in Fig. 1. The motor is fed from two five phase two-level voltage source inverters (VSI) from both the sides of the stator windings. The first inverter (VSI-1) is fed from a DC source while a charged capacitor is provided at the DC-link of the second inverter (VSI-2).

The instantaneous voltage appearing across the different stator phase windings of the FPIM can be obtained using the pole voltages of the two VSIs as

$$V_{xx'} = V_{xo} - V_{x'o'} + V_{oo'} \quad (1)$$

where $x \in (a, b, c, d, e)$,

$$\text{and } V_{oo'} = \sum_{x=a}^e \frac{1}{5} (V_{x'o'} - V_{xo}) \quad (2)$$

where o and o' are the reference points on the negative rail of DC bus of VSI-1 and VSI-2 as shown in Fig. 1. Nevertheless, circulation of any common mode current is naturally prevented, since the DC links of the two VSIs are isolated. The functioning of the VSIs is decoupled in such a way that the VSI-1 delivers only the active power demand of the drive, whereas the VSI-2 delivers the entire reactive power required by the motor in all operating conditions. Thus, the VSI-1 always operates at UPF. Since VSI-2 exchanges only reactive power, it is sufficient to have only a charged capacitor at its DC-link. The VSI-2 functions as a series compensator

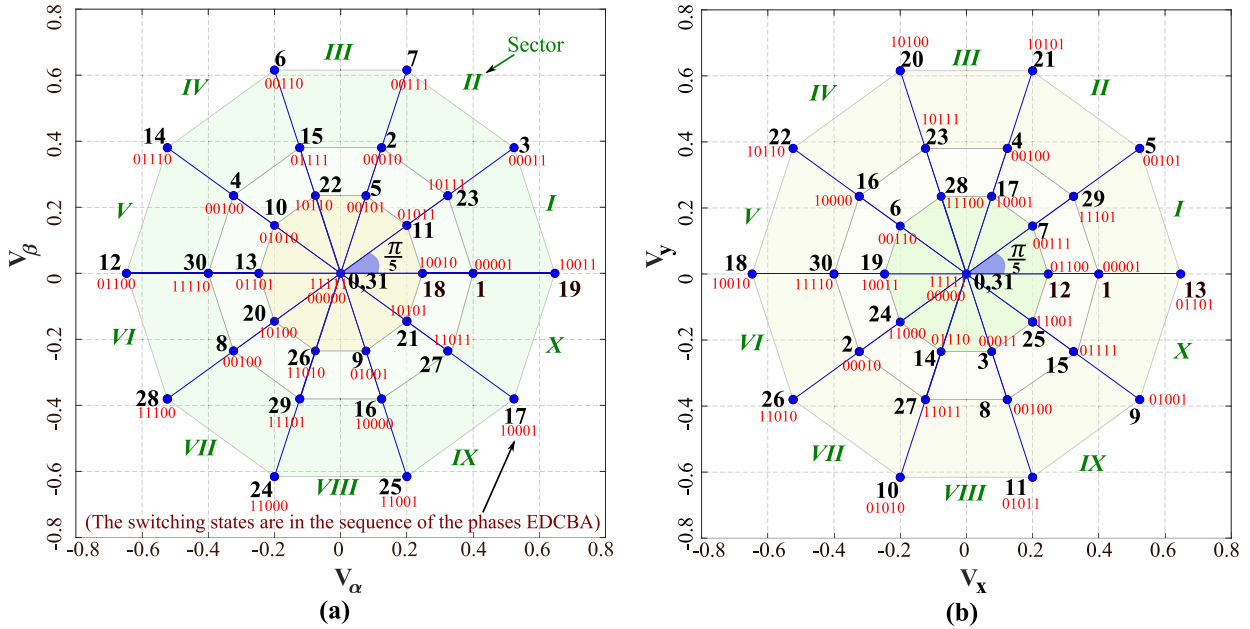


FIGURE 2. Voltage space vector structure of five phase two level VSI in a) fundamental ($\alpha\beta$) plane b) auxiliary (xy) plane. The 5-bit binary numbers adjacent to vector locations represent the switching state of the respective vectors in the phase order ‘EDCBA’, in which ‘1’ and ‘0’ represent the ‘ON’ and ‘OFF’ statuses of the top switch of the respective inverter leg. (The vector magnitudes are in per unit with $V_{DC} = 1$.)

for injecting the voltage required to overcome the reactive voltage drop in the motor that increases with the increase in speed.

This control scheme has the capability to operate the drive much above the base speed compared to a single inverter fed five phase IM drive, having the same DC-link voltage, as described later in this paper. The decoupled control of the two inverters also ensures that the voltage in the harmonic plane is nullified in a switching period.

III. VOLTAGE SPACE VECTOR DECOMPOSITION IN THE FIVE PHASE SPACE VECTOR DOMAIN

A voltage space vector based control scheme is utilized for extension of the constant power speed range of the five phase open-end winding induction motor drive fed by two VSIs, shown in Fig. 1. In this configuration, the resultant of the voltage vectors generated by both VSIs will appear across the motor winding. The voltage space vector structures of a five phase two-level VSI in the fundamental plane and auxiliary plane are shown in Fig. 2. The voltage space vector structures generated by VSI-1 and VSI-2 will be identical in shape, but the vector magnitudes will be scaled according to the respective DC-link voltages. As mentioned earlier, the space vector plane of a five phase inverter consists of two subspaces, namely the $\alpha\beta$, and xy planes, in which the latter corresponds to harmonic voltages that do not contribute to any torque in a machine having distributed winding structure [1], [16].

The voltage space vectors in the $\alpha\beta$ and xy space vector planes, denoted by $V_{\alpha\beta, VSI-1}$ and $V_{xy, VSI-1}$ respectively, associated with VSI-1 can be expressed as

$$V_{\alpha\beta, VSI-1} = [C_{\alpha\beta}] [V_{p1}]^T \quad (3)$$

where $[C_{\alpha\beta}] = [1 e^{jk} e^{j2k} e^{j3k} e^{j4k}]$, and $k = (2\pi/5)$.

$$V_{xy, VSI-1} = [C_{xy}] [V_{p1}]^T \quad (4)$$

where $[C_{xy}] = [1 e^{j3k} e^{j2k} e^{j4k} e^{j2k}]$ and the pole voltage matrix $[V_{p1}] = [V_{ao} V_{bo} V_{co} V_{do} V_{eo}]$.

Similarly, the voltage space vectors associated with VSI-2 in $\alpha\beta$ and xy space vector planes, denoted by $V_{\alpha\beta, VSI-2}$ and $V_{xy, VSI-2}$ respectively, can be obtained by replacing $[V_{p1}]$ from (3), and (4), with pole voltages of VSI-2, $[V_{p2}]$, where $[V_{p2}] = [V_{a'o'} V_{b'o'} V_{c'o'} V_{d'o'} V_{e'o'}]$.
i.e.,

$$V_{\alpha\beta, VSI-2} = [C_{\alpha\beta}] [V_{p2}]^T \quad (5)$$

$$V_{xy, VSI-2} = [C_{xy}] [V_{p2}]^T \quad (6)$$

Now, the voltage space vector that appear across the stator windings of the FPIM is the resultant of the voltage space vectors generated by VSI-1 and VSI-2, given by

$$V_{m, \alpha\beta} = V_{\alpha\beta, VSI-1} - V_{\alpha\beta, VSI-2} \quad (7)$$

$$V_{m, xy} = V_{xy, VSI-1} - V_{xy, VSI-2} \quad (8)$$

where $V_{m, \alpha\beta}$ and $V_{m, xy}$ represents the resultant voltage space vector across the stator in $\alpha\beta$ and xy space vector planes, respectively.

A. FIVE PHASE INDUCTION MOTOR (FPIM) MODEL

The FPIM model can be represented in orthogonal stationary reference frame using the two voltage space vector subspaces ($\alpha\beta$ and xy) [1]. The stator and rotor voltage equations corresponding to the $\alpha\beta$ -plane is given by,

$$V_{m\alpha} = I_{s\alpha} R_s + p\Psi_{s\alpha} \quad (9)$$

$$V_{m\beta} = I_{s\beta}R_s + p\Psi_{s\beta} \quad (10)$$

$$V_{r\alpha} = 0 = I_{r\alpha}R_r + p\Psi_{r\alpha} + \omega_r\Psi_{r\beta} \quad (11)$$

$$V_{r\beta} = 0 = I_{r\beta}R_r + p\Psi_{r\beta} - \omega_r\Psi_{r\alpha} \quad (12)$$

where R_s represents the stator resistance, and I_s represents the stator current vector. The letters α and β in the subscripts denotes the component of the quantity along the respective axis. The variables ψ_s and ψ_r denotes the stator flux linkage phasor and rotor flux linkage phasor, respectively. Similarly, the variable V_r denotes the rotor voltage and I_r represents the rotor current phasor. The variable ω_r denotes the electrical rotor frequency and p represents differential operator (d/dt).

Similarly, the stator and rotor equations corresponding to the xy-plane can be expressed as

$$V_{mx} = I_{sx}R_s + p\Psi_{sx} \quad (13)$$

$$V_{my} = I_{sy}R_s + p\Psi_{sy} \quad (14)$$

$$V_{rx} = 0 = I_{rx}R_r + p\Psi_{rx} \quad (15)$$

$$V_{ry} = 0 = I_{ry}R_r + p\Psi_{ry} \quad (16)$$

The stator and rotor flux linkage terms in (9) to (16) are given as follows. The component of ψ_s and ψ_r in fundamental plane along the axis- k where $k \in (\alpha, \beta)$ is given by,

$$\Psi_{sk} = L_{ss}I_{sk} + L_m I_{rk} \quad (17)$$

$$\Psi_{rk} = L_{rr}I_{rk} + L_m I_{sk} \quad (18)$$

whereas the components of ψ_s in xy-harmonic plane along the axis- n where $n \in (x, y)$ are given by,

$$\Psi_{sn} = L_s I_{sn} \quad (19)$$

where L_{ss} , L_{rr} and L_m represents the self-inductance of the stator, self-inductance of the rotor, and the magnetizing inductance, respectively. L_s denotes the leakage inductance of stator. It may be noted that the harmonic currents in xy-plane do not generate a resultant rotating magnetomotive force [1]. As a result, the back emf and mutual inductance terms are absent in the model of FPIM in xy-plane as given in (13) to (16), and (19).

The effect of these voltage space vectors on the FPIM can be represented using dynamic equations of the FPIM by further elaborating (9) to (19) in the stationary orthogonal $\alpha\beta$ and xy planes as given below:

$$V_{m,\alpha\beta} = R_s I_s + \sigma L_{ss} \frac{dI_s}{dt} - \frac{L_m}{L_{rr}} R_r I_r + j \frac{L_m}{L_{rr}} \omega_r \psi_r \quad (20)$$

$$V_{m,xy} = R_s I_{s,xy} + L_s \frac{dI_{s,xy}}{dt} \quad (21)$$

where $\sigma = 1 - \frac{L_m^2}{L_{ss}L_{rr}}$, is the leakage factor.

From (21), it is evident that, since the voltage produced in the xy-plane is not counteracted by the back EMF, it can cause circulation of large harmonic currents and consequent losses in the system [1]. Hence it is required to nullify the average voltage generated in the auxiliary plane in a switching period

while generating the required voltage vector in the fundamental plane. This can be effectively achieved using space vector decomposition, followed by a space vector modulation scheme as explained next.

B. SPACE VECTOR DECOMPOSITION

The harmonic voltages in the auxiliary space vector plane are nullified, as discussed in the previous section, by using virtual voltage vectors. Therefore, the space-vector quantities mentioned in this paper hereafter belongs to $\alpha\beta$ -plane, unless specified otherwise. Let V_m be the reference voltage vector obtained from the speed control algorithm to be realized across the stator of the FPIM. This reference voltage space vector V_m is decomposed into two virtual vector components namely V_{VSI-1} and V_{VSI-2} . The voltage vector V_{VSI-1} , and V_{VSI-2} are then used as the reference vectors to be generated in VSI-1 and VSI-2 in $\alpha\beta$ -plane, respectively, so that they result in V_m across the stator windings, as given by (7). i.e.,

$$V_{\alpha\beta,VSI-1} = V_{VSI-1} \quad (22)$$

$$V_{\alpha\beta,VSI-2} = V_{VSI-2} \quad (23)$$

Therefore, by substituting (22), and (23) in (7), the voltage vector generated in $\alpha\beta$ -plane becomes:

$$V_{m,\alpha\beta} = V_{VSI-1} - V_{VSI-2} = V_m \quad (24)$$

In order to make sure that the VSI-2 exchanges only reactive power with the motor, it has to be ensured that there is a phase shift of 90° (ideally) between the motor current vector (denoted by I_s) and the voltage vector produced by VSI-2 (V_{VSI-2}). On the other hand, the voltage vector generated by VSI-1 (V_{VSI-1}) should be in phase with I_s to make sure that the entire active power required by the system is supplied by VSI-1, which is fed from a DC source. Consequently, there must be a phase shift of 90° between the voltage vectors generated by VSI-1 (V_{VSI-1}) and VSI-2 (V_{VSI-2}) under ideal condition, as the same current flows through both inverters.

The realization of an arbitrary reference voltage vector V_m in the motor winding is illustrated in Fig. 3a. The DC-link voltages of the two VSIs are assumed to be different, as represented in Fig. 3a by using two similar but scaled versions of the five phase 2-level space vector structure in $\alpha\beta$ -plane. For instance, let the stator current I_s be aligned along α -axis, and the reference voltage V_m be at an angle 36° from the α -axis. Now, two virtual voltage vectors V_{VSI-1} and V_{VSI-2} are generated in VSI-1, VSI-2 respectively to generate V_m across the stator in $\alpha\beta$ -plane, while ensuring cancellation of xy-plane voltage harmonics, as described in the next subsection.

C. ELIMINATION OF XY-PLANE VOLTAGE HARMONICS USING VIRTUAL VOLTAGE VECTORS FROM INDIVIDUAL INVERTERS

As already explained, V_{VSI-1} must be in phase with the stator current. Hence, the virtual voltage vector V_{VSI-1} is generated in VSI-1 along α -axis, in average sense over the

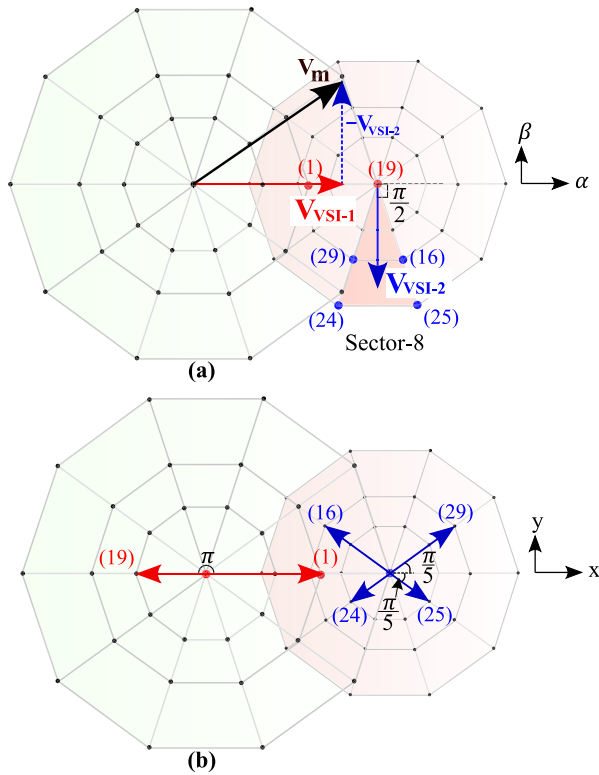


FIGURE 3. Voltage vector decomposition in a) $\alpha\beta$ -plane to generate the reference voltage vector V_m . b) Mapping of the selected active vectors in xy -harmonic voltage plane.

sampling period as shown in Fig. 3a. The active vectors ‘19’ and ‘1’ along with zero vector are used to realize V_{VSI-1} . During the same sampling interval, a virtual voltage vector V_{VSI-2} is generated in VSI-2 at the middle of sector-8 (Fig. 3a), with a phase shift of 90° with respect to V_{VSI-1} as shown in Fig. 3a, using the large voltage vectors ‘24’ and ‘25’ and medium vectors ‘16’ and ‘29’ along with zero vectors. This phase relationship is maintained between the virtual voltage vectors generated by VSI-1 and VSI-2 under all operating conditions. Thus, any voltage vector can be generated in a virtual manner across the motor windings in $\alpha\beta$ -plane in a similar way by applying two orthogonal virtual voltage vectors of VSI-1 and VSI-2.

On the other hand, from Fig. 2a and Fig. 2b, it can be seen that the large voltage vectors ‘24’ and ‘25’ and the medium vectors ‘16’ and ‘29’ used for generation of V_{VSI-2} in the $\alpha\beta$ -plane are mapped in the opposite directions in the xy -plane. This feature is depicted in Fig. 3b. Similarly, the vectors 19 and 1 used for generating V_{VSI-1} in $\alpha\beta$ -plane, are mapped as opposite vectors in xy -plane.

Therefore, the average voltage in the auxiliary plane is made zero in a switching period by controlling the dwell times of the active vectors [16], [17]. The dwell times of large and medium vectors are applied in the ratio of their magnitudes. i.e., 0.618:0.382 [16]. When a virtual voltage vector is to be generated inside a sector, two large vectors and two medium vectors forming that sector are used along

with zero vectors. This implies,

$$V_{xy, VSI-1} = 0 \tag{25}$$

$$V_{xy, VSI-2} = 0 \tag{26}$$

This results in nullification of resultant voltage vector $V_{m,xy}$ generated across the stator in xy -plane as per (8) in an average sense over a switching period. Consequently, the non-torque producing harmonic voltages (of order 3, 7, 13 etc.) are significantly suppressed, while realizing the required resultant reference voltage vectors in the $\alpha\beta$ -plane, as demonstrated in the results section (section-V).

IV. PRINCIPLE OF OPERATION AND BLOCK DIAGRAM OF THE CONTROL SCHEME

The reference voltage vector to be applied on the motor (V_m) (in $\alpha\beta$ -plane) will be given by the speed control algorithm, based on the operating conditions of the drive. The extraction of voltage vector components corresponding to the active and reactive power, and the control of VSIs are carried out based on a synchronously revolving reference frame oriented with the stator current vector. For this purpose, the angular position of the stator current space vector is identified first. The stator current space vector I_s (in $\alpha\beta$ -plane) can be obtained from the five phase stator currents using the transformation matrix given below in (27):

$$I_s = [C_{\alpha\beta}] [I_s]^T = I_{s\alpha} + jI_{s\beta} \tag{27}$$

where $[I_s] = [i_{sa}i_{sb}i_{sc}i_{sd}i_{se}]$, represents the stator currents through the five stator phase windings, and the matrix $[C_{\alpha\beta}]$ represents the five phase to $\alpha\beta$ transformation as given in (3). $I_{s\alpha}$ and $I_{s\beta}$ represents the stationary orthogonal components of I_s in fundamental ($\alpha\beta$) plane.

Next, a synchronously revolving dq-reference frame is defined in such a way that, the d -axis is aligned along the stator current vector I_s , and the q -axis leads the d -axis by 90° , as shown in Fig. 4a. Subsequently, the reference voltage vector, V_m that is currently defined in $\alpha\beta$ -reference frame is transformed into the dq-reference frame using Park’s transformation. The two dq-reference frame components V_d and V_q , are defined by equations (28) and (29) given below and depicted in Fig. 4a.

$$V_m = V_d + jV_q \tag{28}$$

$$\text{where } \begin{bmatrix} V_d \\ V_q \end{bmatrix} = \begin{bmatrix} \cos \theta_i & \sin \theta_i \\ -\sin \theta_i & \cos \theta_i \end{bmatrix} \begin{bmatrix} V_{m\alpha} \\ V_{m\beta} \end{bmatrix} \tag{29}$$

in which θ_i represents the instantaneous angular position of I_s , and the terms $V_{m\alpha}$ and $V_{m\beta}$ represent the components of V_m along α -axis and β -axis, respectively. The trigonometric terms involved in (29) can be obtained from (27), as

$$\cos \theta_i = \frac{I_{s\alpha}}{\sqrt{(I_{s\alpha}^2 + I_{s\beta}^2)}}, \text{ and } \sin \theta_i = \frac{I_{s\beta}}{\sqrt{(I_{s\alpha}^2 + I_{s\beta}^2)}}. \tag{30}$$

Now, any voltage component along the d -axis is responsible for real power transfer in the drive as it is in phase with the stator current vector. On the other hand, any voltage

component along the q -axis (which is in quadrature with I_s), is responsible for reactive power transfer. Therefore, the two components of the stator voltage reference vector, i.e., V_d and V_q represent the voltages corresponding to the active power requirement and the reactive power requirement of the motor, respectively. Thus, the stator current reference frame is used for the decoupling of active and reactive voltage components of the stator reference voltage vector effectively. These voltage components constitute the references for the operation of VSI-1 and VSI-2 as explained in the following subsections.

A. COMPUTATION OF REFERENCE VOLTAGES OF MAIN VSI AND CAPACITOR FED VSI IN DQ- REFERENCE FRAME

The voltage vectors to be generated by VSI-1 and VSI-2, i.e., V_{VSI-1} and V_{VSI-2} , are also resolved along the stator current reference frame axes d , and q . i.e.,

$$V_{VSI-1} = V_{VSI-1,d} + jV_{VSI-1,q} \quad (31)$$

$$V_{VSI-2} = V_{VSI-2,d} + jV_{VSI-2,q} \quad (32)$$

As described earlier, the real parts, $V_{VSI-1,d}$, $V_{VSI-2,d}$ are the voltage components of VSI-1 and VSI-2, respectively, that result in real power transfer. On the other hand, the q -axis voltage components associated with VSI-1, and VSI-2, i.e., $V_{VSI-1,q}$, and $V_{VSI-2,q}$ result in reactive power transfer. From (24), (28), (31), and (32), the voltage components corresponding to real, and reactive power demanded by the motor (given by the speed and torque control algorithm), and that generated by the VSIs can be related as:

$$V_d = V_{VSI-1,d} - V_{VSI-2,d} \quad (33)$$

$$V_q = V_{VSI-1,q} - V_{VSI-2,q} \quad (34)$$

As mentioned before, the capacitor-fed VSI (VSI-2) supports the entire reactive power requirement of the drive and does not take part in any real power transfer. Therefore, ideally, the d -axis reference voltage of VSI-2 ($V_{VSI-2,d}$) in (32) can be set to zero. Consequently, the capacitor voltage at the DC-link of VSI-2 would naturally be maintained at a stable level under ideal conditions. The voltage and current phasors during this ideal condition is shown in Fig. 4a.

However, practically, the capacitor voltage at the DC-link of VSI-2 will drop due to non-idealities such as losses in the inverter and the capacitor. As a result, VSI-2 will not be able to provide the voltage output necessary to support the required reactive power.

To overcome this problem, VSI-2 will have to be provided with a small amount of active power to compensate for the losses in the capacitor and the inverter, so that the capacitor voltage can be maintained at the desired level [9], [10], and [13]. For this, the reference voltages of the VSIs are modified as described in the next subsection.

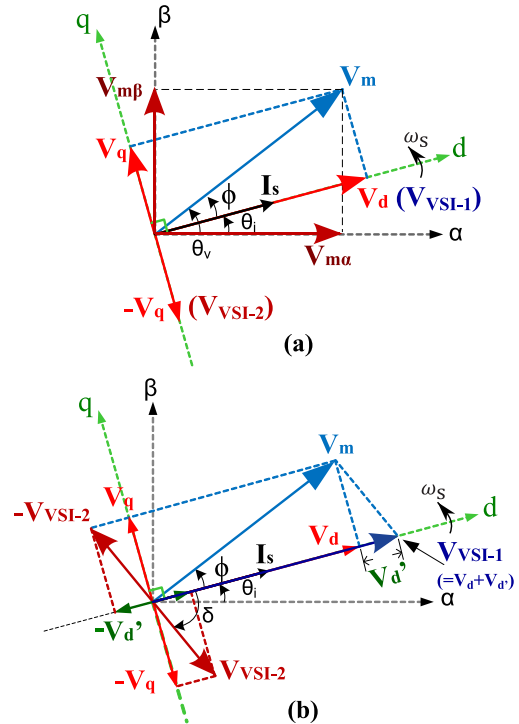


FIGURE 4. The reference stator voltage vector V_m , stator current vector I_s , and VSI-1 and VSI-2 reference voltages in $\alpha\beta$ and dq reference frames, under a) ideal condition, and b) practical condition where VSI-2 draws active power from VSI-1 to compensate for the losses to maintain the DC-link capacitor voltage at the reference value.

B. CONTROL OF VSI-2 FOR REACTIVE POWER SUPPORT, AND DC- LINK CAPACITOR VOLTAGE REGULATION

The d -axis voltage component of VSI-1 represents the voltage component in phase with the stator current, and hence contributes to supply of active power to the drive. Also, the d -axis voltage component of VSI-2 represents the absorption of active power by VSI-2 to compensate for the losses and thereby ensuring that the capacitor voltage at VSI-2 is maintained at the required level. Let this d -axis voltage component be V'_d . Thus,

$$V_{VSI-2,d} = V'_d \quad (35)$$

On the other hand, the q -axis component of the voltage to be produced by VSI-2 is set to be equal to the q -axis component of voltage demanded by the motor, i.e., V_q (from (28)). This ensures that the entire reactive power requirement of the motor is supported solely by VSI-2. Or, in other words, VSI-1 need not generate any voltage component along q -axis, i.e., $V_{VSI-1,q}$ is zero in (34). Therefore, to generate voltage V_q across the stator along q -axis, as per (34),

$$V_{VSI-2,q} = -V_q \quad (36)$$

Hence, by substituting (35) and (36) in (32), the reference voltage vector of VSI-2, V_{VSI-2} is obtained as:

$$V_{VSI-2} = V'_d - jV_q \quad (37)$$

The effect of V'_d appears in the voltage space vectors as given in Fig. 4b. It is clear that the angle (marked as δ

in Fig. 4b) between the voltage space vector generated by VSI-2 (V_{VSI-2}) and the stator current I_s is no longer 90° . Instead, δ will be less than 90° , leading to the generation of the component V_d' , that is used for compensating the losses in the inverter and the capacitor. The voltage vector components of VSI-1 and VSI-2 in the stator current reference frame (dq) are depicted in Fig. 5.

The d -axis voltage reference of VSI-2 (V_d') is obtained from the output of the PI controller used for capacitor voltage control. Since the VSI is operated in voltage controlled mode, a reference to draw adequate amount of active power should be given as a voltage component. Hence, the output of the capacitor voltage PI controller is treated as a voltage reference in the control scheme presented in Fig. 6, even though what happens effectively during the switching of the VSI is the flow of charging or discharging current through the capacitor in order to maintain the voltage across it at its reference value. Thus, the output of the PI controller gives the d -axis voltage reference (V_d') of VSI-2.

The capacitor voltage reference (V_{cap}) is set based on the maximum reactive power (Q^*) requirement of the drive in the extended speed range. The Q^* includes the reactive power absorbed by the motor reactance which increases substantially due to the increased frequency of the applied voltage, at higher speeds. The determination of the capacitor voltage reference is explained later in this paper in subsection-D.

Since a series reactive power compensation scheme is employed here, in which the motor current is taken as the reference, the increase in reactive power reflects in the increased fundamental component of voltage to be generated by VSI-2. The capacitor fed VSI-2 injects a voltage to overcome the increased stator reactive voltage drop due to the increase in frequency, there by extending the constant power speed region, which is constrained by the DC power source voltage in the conventional drives.

C. CONTROL OF MAIN VSI (VSI-1)

Since the active power requirement of the drive is supplied entirely from VSI-1, the active power delivering component of VSI-1 voltage ($V_{VSI-1,d}$) must be set equal to that of d -axis reference stator voltage (V_d) in ideal case. However, as described earlier, a small active power is absorbed by the VSI-2 for maintaining its DC-link capacitor voltage at the required level. Therefore, VSI-1 must also deliver this small active power component in addition to the active power required by the motor. Therefore, the d -axis component of voltage reference of VSI-1 now consists of

$$V_{VSI-1,d} = V_d + V_d' \quad (38)$$

As discussed earlier, VSI-1 is not involved in supply of reactive power to the motor. Hence the q -axis voltage reference of VSI-1 (i.e., $V_{VSI-1,q}$) that is responsible for reactive power transfer is set as zero. i.e.,

$$V_{VSI-1,q} = 0 \quad (39)$$

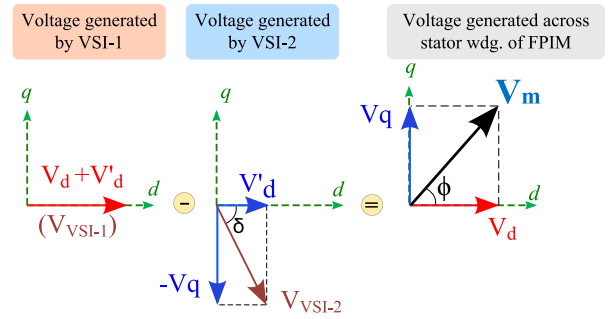


FIGURE 5. Voltage vector components generated by VSI-1 and VSI-2 along d -axis and q -axis in stator current reference frame (I_s along d -axis), to realize the reference voltage vector V_m across the stator winding of FPIM.

Hence, by substituting (38) and (39) in (31), the reference voltage vector of VSI-1 is obtained as:

$$V_{VSI-1} = (V_d + V_d') + j0 \quad (40)$$

The reference voltage vector components of VSI-1 and VSI-2 along the d , and q axes, and the formation of reference stator voltage vector V_m in stator current reference frame (dq-frame) are shown separately in Fig. 5.

The complete block diagram of the proposed control scheme is shown in Fig. 6. The reference voltage $V_m \angle \theta_V$ that must be applied across the motor is given by the motor control algorithm, where θ_V represents the angular position of reference stator voltage vector V_m from α -axis of the $\alpha\beta$ -plane. The constant volts per hertz control is used for generating the reference voltage vector in this work. The other control schemes like the field oriented control (FOC) can also be used for generation of the reference voltage vector without affecting the overall control structure. The reference voltage vector generated by the motor control algorithm is converted into the stationary two-axis reference frame components $V_{m\alpha}$ and $V_{m\beta}$ using five-phase to two-phase (fundamental plane) Clarke's transformation. Then, Park's transformation is applied to convert $V_{m\alpha}$ and $V_{m\beta}$ to the synchronously rotating stator current (dq) reference frame, as given by (29). The unit vectors ($\cos \theta_i$ and $\sin \theta_i$) required for the Park's transformation are derived from stationary reference frame components $i_{s\alpha}$ and $i_{s\beta}$ of I_s , (as given by (30)) as shown in Fig. 6. The voltage vector components corresponding to active and reactive power are then generated as described previously in this paper. These reference components are then converted back to $\alpha\beta$ -plane and then realized using SVPWM scheme incorporating the elimination of xy -plane voltages.

D. OPERATION IN THE EXTENDED SPEED REGION

The operation of the drive in the extended speed range can be explained with the help of the equivalent circuit (per phase) of the five phase induction motor drive with open end stator windings powered from a DC source fed inverter at one side of the windings and a capacitor fed inverter from the other side, shown in Fig. 7. Due to the orthogonal relationship between the fundamental components of the output voltages

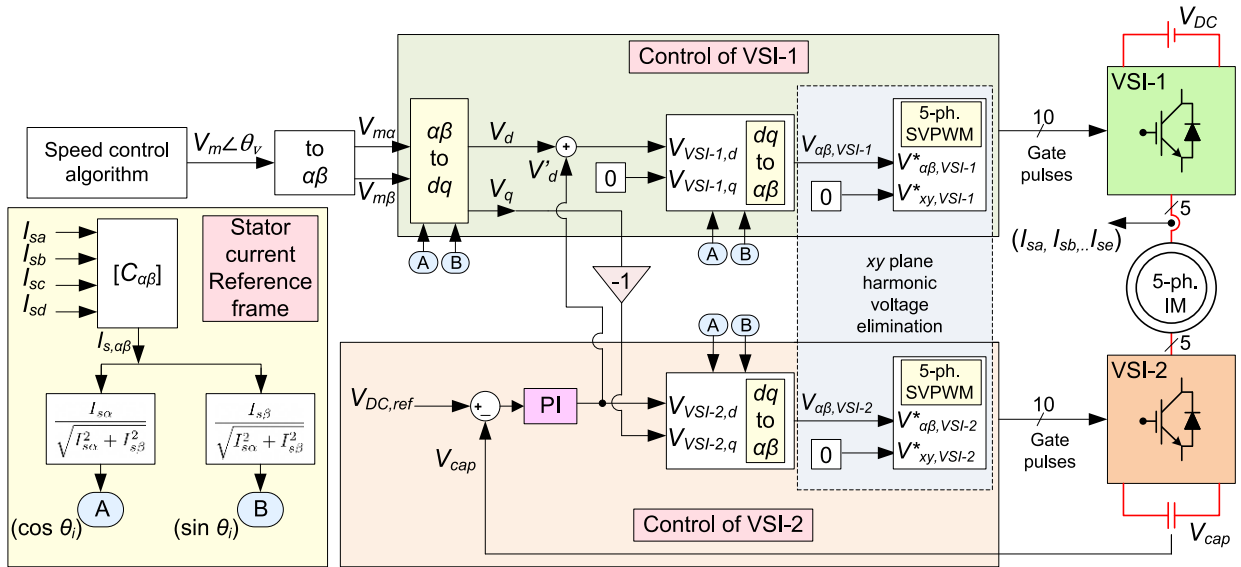


FIGURE 6. Block diagram of over-all control scheme of the proposed speed range extension scheme of five phase open-end winding IM drives.

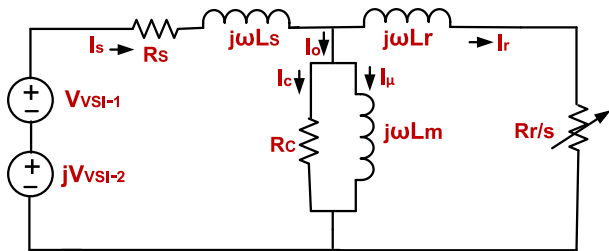


FIGURE 7. Steady state equivalent circuit (per phase) of the dual inverter fed five phase induction motor drive shown in Figure-1.

of VSI-1 and VSI-2 they are represented as V_{VSI-1} and jV_{VSI-2} , respectively.

Active power supplied by the VSI-1 can be expressed as

$$I_s^2 R_s + I_c^2 R_c + \frac{I_r^2 R_r}{s} + P_{VSI\ loss} = V_{VSI-1} I_s \quad (41)$$

Reactive power supplied by the VSI-2 can be expressed as:

$$j\omega L_s I_s^2 + j\omega L_m I_\mu^2 + j\omega L_r I_r^2 = jV_{VSI-2} I_s \quad (42)$$

In the equations (41) and (42), R_s and R_r are the stator and rotor resistances respectively, R_c is the resistance representing the core loss, 's' is the slip, ' ω ' is the supply frequency corresponding the operating speed, L_s and L_r are the stator and rotor leakage inductances respectively, L_m is the magnetizing inductance, I_μ is the magnetizing current and I_c is the core loss component of the stator current. The variable $P_{VSI\ loss}$ represents the total losses in the two VSIs and the capacitor.

It is evident from (42) that the reactive power requirement of the drive increases with speed since the frequency ' ω ' increases. This increase in reactive power requirement will be substantial in the extended speed region mainly because of the significant increase in the reactive voltage drops across the leakage inductances. The capacitor fed inverter VSI-2 compensates this reactive voltage drop which increases with the

speed by injecting a reactive voltage in series, thus relieving the VSI-1 from this task.

Hence, the output voltage that can be realised from VSI-1 at the end of linear modulation range will not be utilised fully even when the drive operates at the base speed with rated load, compared to a single inverter fed drive operating with the same DC source voltage under similar conditions. The unused voltage capability of VSI-1 can be utilised for overcoming the increased back EMF when the drive operates above the base speed. Thus VSI-1 and VSI-2 together facilitate the extension of speed range above the base speed, in the constant power region, without field weakening.

The capacitor voltage V_{cap} of VSI-2 is set such that VSI-2 will be able to provide the voltage output necessary to support the peak reactive power requirement of the motor at its maximum extended speed with full load. The reference voltage of the capacitor can be determined as follows.

The maximum fundamental phase voltage output (rms) obtainable from the capacitor-fed two-level five phase VSI (VSI-2) under linear modulation range using the space vector PWM scheme with xy-plane harmonic voltage elimination is given by [16]:

$$|V_{VSI-2}| = 0.525 \frac{V_{cap}}{\sqrt{2}} \quad (43)$$

where V_{cap} is the DC-link capacitor voltage.

Considering the nearly orthogonal current and voltage of the VSI-2, if $I_{s,RMS}$ is the RMS value of the rated stator current, and assuming the operation of VSI-2 at the end of linear modulation range, the reactive power (Q^*) can be expressed as:

$$Q^* = 5 * \left(\frac{0.525}{\sqrt{2}} V_{cap} \right) I_{s,RMS} \quad (44)$$

The peak reactive power requirement (Q^*) of the FPIM drive in its extended speed range can be determined using

TABLE 1. Five phase induction motor parameters.

Parameter	Value
Power Rating	0.75 kW
Poles	4
Stator resistance	1.92 Ω
Rotor resistance	1.43 Ω
Mutual inductance	196 mH
Stator leakage inductance	8.66 mH
Rotor leakage inductance	8.66 mH

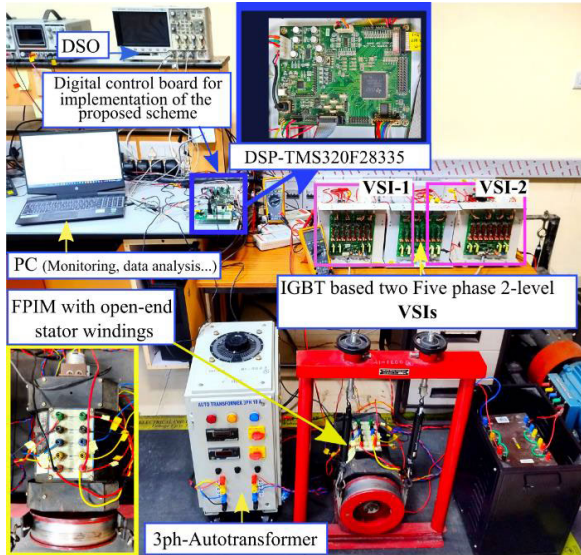


FIGURE 8. Experimental setup for verifying and validating the proposed scheme.

the motor parameters as given in equation (42). The capacitor voltage can then be calculated from (44) as follows:

$$V_{cap} = \frac{\sqrt{2}Q^*}{5 * 0.525 I_{s,RMS}} \quad (45)$$

However, the resultant voltage appearing across the stator could impose a limitation on the maximum speed ω_{max} based on the maximum voltage capability of the motor, V_{max} . i.e.,

$$V_{max}^2 \geq (V_{VSI-1,\omega_{max}}^2 + V_{VSI-2,\omega_{max}}^2) \quad (46)$$

where $V_{VSI-1,\omega_{max}}$ and $V_{VSI-2,\omega_{max}}$ represents the voltages corresponding to the condition ω_{max} .

It may be noted that in addition to the limitations imposed by the stator voltage constraints, the mechanical stress on the motor components such as the rotor, shaft, and bearing etc. could also limit the maximum speed of the drive.

V. EXPERIMENTAL RESULTS AND DISCUSSION

The proposed scheme is verified experimentally on a laboratory prototype, consisting of a five-phase induction motor with open-end stator windings, shown in Fig. 8. The motor parameters are given in Table 1. The induction motor is fed from two 2-level five phase VSIs consisting of SKM100GB12T4 IGBT modules. The DC-link voltage was

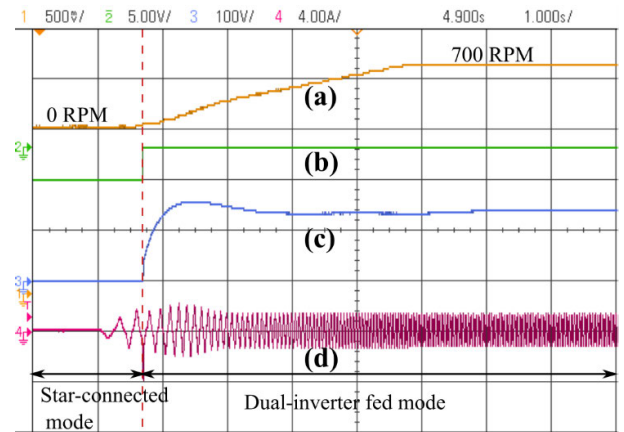


FIGURE 9. Experimental result: startup and acceleration from 0 to 700 RPM at no load. a) speed (560 RPM/div) b) mode selection command c) VSI-2 DC-link Capacitor voltage (100 V/div.) d) stator phase-A current (4 A/div.). X-axis scale: 1 s/div.

set at 150 V, and the corresponding base speed of the motor is 400 RPM. Hall effect voltage and current sensors are used for measuring DC-link voltages and stator phase currents. The control scheme is implemented using TMS320F28335 digital signal controller from Texas Instruments. Experimental results are obtained for steady state and transient operating conditions of the drives.

Fig. 9 shows the start-up and acceleration of the drive from 0 RPM to 700 RPM i.e., above the base speed. The motor is in star-connected configuration till 140 RPM, and then it is switched to dual inverter-fed mode as indicated in trace-b of Fig. 9. Fig. 10 shows the charging of the capacitor of VSI-2 to the reference value of 140 V (trace-b) during the acceleration of the drive from 0 RPM to 700 RPM. The PI controller maintains the capacitor voltage at the reference value and limits overcharging during the dynamic operation of the motor. The reactive power requirement of the drive increases with the increase in speed. This increase is reflected in the modulation index of VSI-2, as shown in trace-c of Fig. 10, indicating the increase in fundamental component of the output voltage of the inverter.

The voltage across stator winding phase-A, the fundamental component of phase voltages of VSI-1 and VSI-2 corresponding to stator winding phase-A, and stator current in phase-A are shown in trace-a, trace-b, trace-c and trace-d in Fig. 11, respectively.

It is evident from Fig. 11 that the phase- A voltage of VSI-1 (Trace-b of Fig. 11) is in phase with stator-phase-A current (Fig. 11, trace-d), showing that VSI-1 is operating at UPF, delivering the entire active power required by the drive. Also, it is clear that the phase-A voltage of VSI-2 (trace-c of Fig. 11) is in quadrature, i.e., lagging the current by 90° with respect to stator phase-A current. This indicates that the reactive power requirement by the drive is provided entirely by the VSI-2. The reactive power requirement of the drive is more than the active power requirement under no-load which

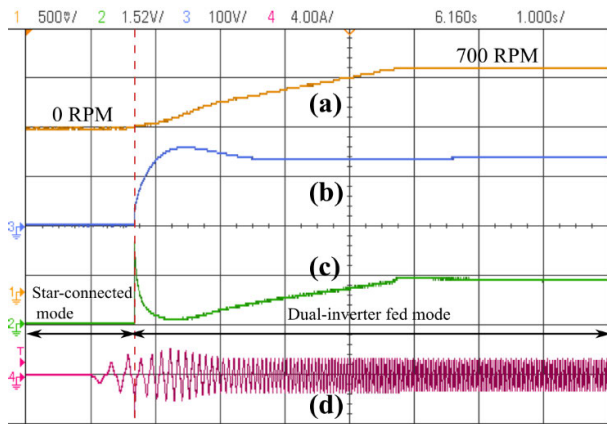


FIGURE 10. Experimental result: startup and acceleration from 0 to 700 RPM at no-load. a) Speed (560 RPM/div.) b) VSI-2 DC-link Capacitor voltage (100 V/div.) c) Modulation index of VSI-2 (0.65 /div.) d) Stator phase-A current (4 A/div.). X-axis scale: 1 s/div.

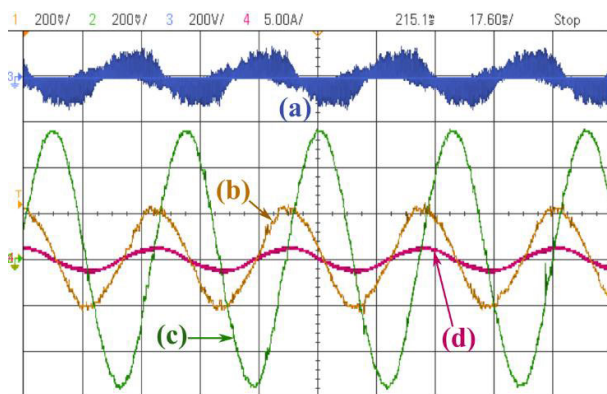


FIGURE 11. Experimental result: Steady-state at 700 RPM and no-load. a) Voltage across stator phase-A (200 V/div.) b) Fundamental component of phase-A voltage of VSI-1 (12 V/div.) c) Fundamental component of phase-A voltage of VSI-2 (12 V/div.) d) Stator phase-A current (5 A/div.). X-axis scale: 17.6 ms/div.

makes the amplitude of fundamental component of VSI-2 phase voltage greater than that of VSI-1 in Fig. 11.

The voltage across stator winding in phase A, FFT of this voltage and the current in the same phase are shown in Fig. 12 for steady state operation at 700 RPM, when the fundamental frequency is 25 Hz. It can be seen that low order harmonics, especially the non-torque producing auxiliary plane voltage harmonics like 3rd and 7th harmonic voltages are negligible and the major harmonic components are appearing at the switching frequency of 4 kHz. It may be noted that the 3rd harmonic content in the phase voltage could have been significant if the conventional space vector switching scheme using the nearest two largest vectors described in [17] was used here for the five phase VSIs.

The effectiveness of the space vector based switching scheme adopted in the proposed system in suppressing the lower order xy-plane voltage harmonics is further showcased in Fig. 13. The phase voltage output of a five phase two-level VSI and its frequency spectrum while adopting the conventional switching scheme by using two nearest large voltage vectors (to realize the reference vector in fundamental plane) is shown in Fig. 13a. Though the SVPWM scheme

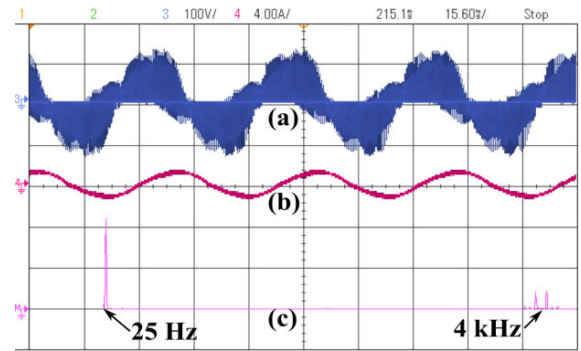


FIGURE 12. Experimental result: Steady state at 700 RPM (25 Hz), no load a) stator phase-A voltage (100 V/div) b) stator phase-A current (4 A/div) c) FFT of stator phase-A voltage. X-axis scale=15.6 ms/div.

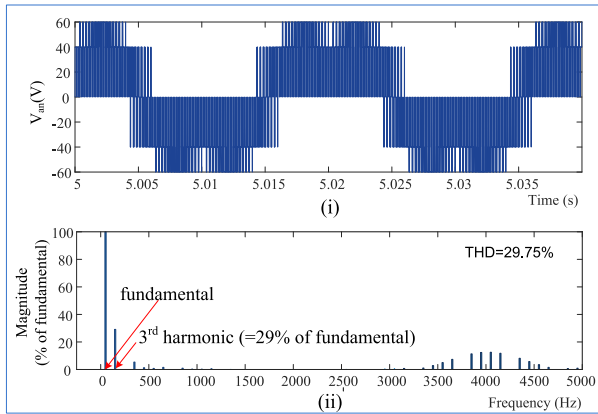
shown in Fig. 13a was carried out with a switching frequency of 4 kHz (as clear from trace-ii of Fig. 13a, where the switching frequency harmonics are visible at 4 kHz.), it is evident that there is a considerable amount of lower order harmonics (for example 3rd harmonic is of magnitude $\approx 29\%$ of fundamental).

On the other hand, the frequency spectrum of the phase voltage of five phase 2-level VSI using the switching scheme adopted in the proposed scheme is shown in Fig. 13b. It is evident that the dominant harmonics appear only at the switching frequency of 4 kHz. It can be seen that the 3rd harmonic is reduced to 1.37% i.e., a reduction by 95.27% is obtained. This shows the effectiveness of the switching scheme used in the proposed scheme to significantly suppress the xy-plane harmonic components at the stator voltage. This validates the effectiveness of the proposed scheme in eliminating the xy-voltage plane harmonics.

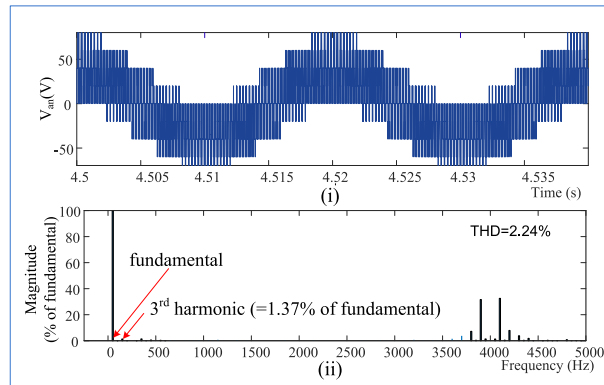
Additionally, the frequency spectrum of stator phase- A current under no load condition is shown in Fig. 14. The THD of stator current waveform provided in [12] with and without harmonic suppression were 14.41%, and 5.50%, respectively. On the other hand, the THD of current waveform obtained in the proposed scheme is 3.50% as shown in Fig. 14. Therefore, compared to the THD without harmonic suppression in [12], the proposed scheme provides 75.71% reduction in THD.

However, it may be noted that a direct quantitative comparison between the harmonic contents of stator currents obtained in the proposed scheme and that obtained in [12] would not be very effective since the harmonic profile of the currents could vary considerably depending on the motor parameters (even if same voltages were applied) and operating conditions. Nevertheless, the results shown in Fig. 12, Fig. 13 and Fig. 14 are insightful in terms of showcasing the effectiveness of the space vector based switching method adopted in the proposed scheme in terms of harmonic suppression.

The angle between voltage vectors generated in the DC source fed inverter VSI-1 and the capacitor fed inverter VSI-2 is depicted in trace- a and trace-b of Fig. 15. It can be seen that the two VSIs are operating with a phase shift of 82.4°. As previously stated, this phase shift is less than 90° as VSI-2



(a)



(b)

FIGURE 13. Frequency spectrum of phase voltage obtained from a five phase two-level VSI using a) Conventional SVPWM scheme using nearest two large vectors per sampling period (without xy-plane harmonic elimination) b) SVPWM scheme using combination of medium and large voltage vectors (with xy-plane harmonic elimination). i) phase voltage ii) FFT of the phase voltage. (Fundamental frequency = 50 Hz, switching frequency = 4 kHz)

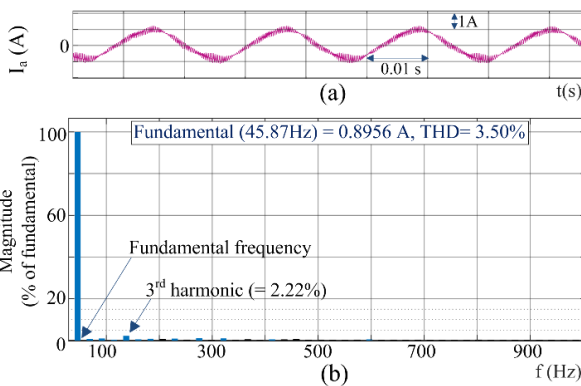


FIGURE 14. Experimental results: steady state operation at 1350 RPM and no load: a) Stator -A phase current and b) Frequency spectrum of stator phase-A current.

is consuming a small amount of active power to compensate for losses in order to keep capacitor voltage at the reference value.

The steady-state speed, the fundamental components of the phase voltages of VSI-1 and VSI-2 corresponding to the stator winding phase-A and the stator current in phase-A, at 1.5 Nm

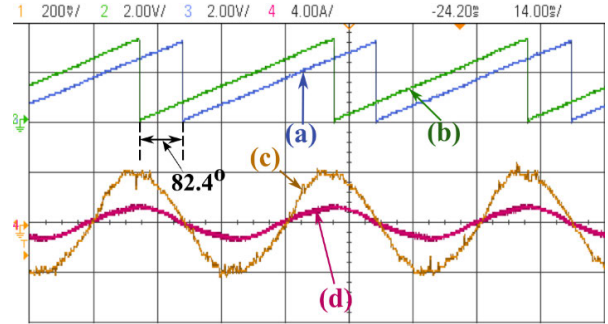


FIGURE 15. Experimental result: Steady state operation at 700 RPM. a) Angle of the voltage vector generated in VSI-2 b) Angle of the voltage vector generated in VSI-1 (w.r.t α - axis) c) Fundamental component of phase-A voltage of VSI-1 (12 V/div.) d) Stator phase-A current (4 A/div.) X-axis scale=14 ms/div.

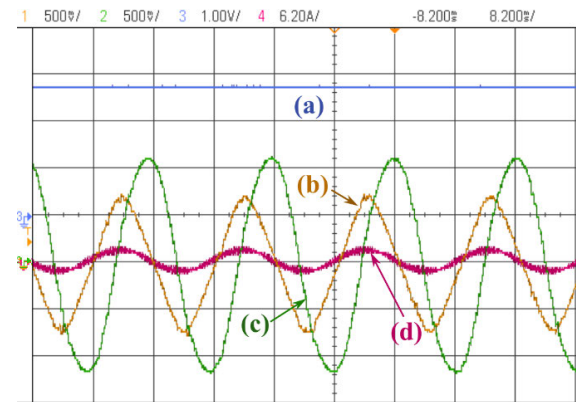


FIGURE 16. Experimental result: steady state 1900 RPM at 1.5 Nm load. a) speed (704 RPM/div.) b) fundamental component of phase-A voltage of VSI-1 (30 V/div.) c) fundamental component of phase-A voltage of VSI-2 (30 V/div.) d) stator phase-A current (6.2 A/div.) X-axis scale: 8.2 ms/div.

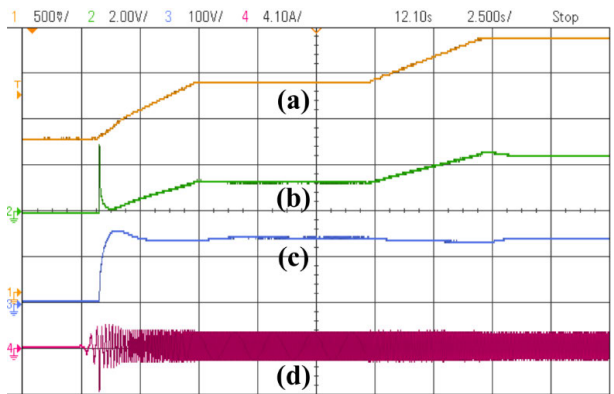


FIGURE 17. Experimental result: acceleration from 0 RPM to 700 RPM and then to 1400 RPM at no load a) speed (560 RPM/div.) b) modulation index of VSI-2 (0.84 /div.) c) VSI-2 DC-link capacitor voltage (100 V/div.) d) stator phase-A current (4.1 A/div.) X-axis scale: 2.5 s/div.

-load, when the drive operates at 1900 RPM (4.75 times the base speed), are shown in Fig. 16.

It is evident from Fig. 16 that the phase-A voltage of VSI-1 (trace-b) is in phase with stator current in phase-A (trace-d), confirming that VSI-1 is operating at unity power factor, delivering the active power required by the drive and thereby forcing the VSI-2 to supply the entire reactive power requirement of the system, which includes the reactive

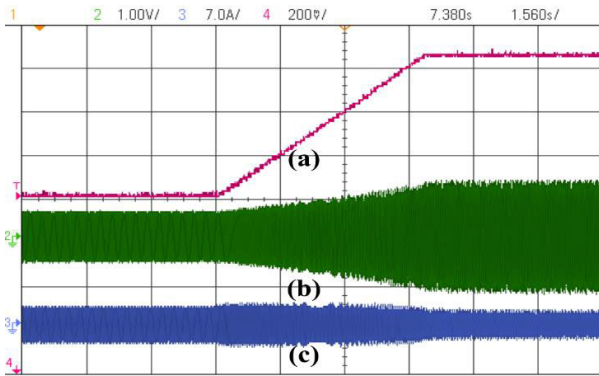


FIGURE 18. Experimental result: Acceleration from 1000 RPM to 1900 RPM at 1.5 Nm load. a) Speed (282 RPM/div.) b) fundamental component of phase-A voltage of VSI-2 (55 V/div.) c) stator phase-A current (7 A/div.). X-axis scale: 1.56 s/div.

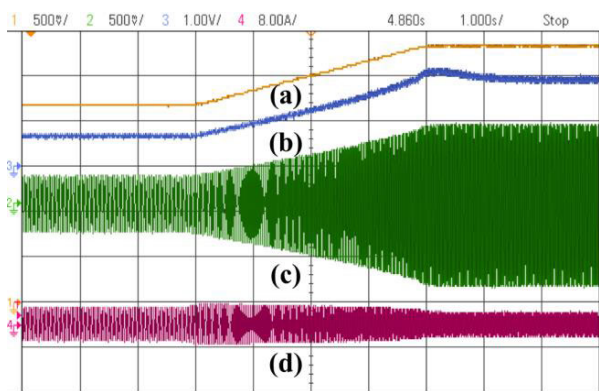


FIGURE 19. Experimental result: acceleration from 1000 RPM to 1900 RPM at 1.5 Nm load a) speed (750 RPM/div.) b) modulation index of VSI-2 (0.84/div.) c) fundamental component of phase-A voltage of VSI-2 (110 V/div.) d) stator phase-A current (8 A/div.). X-axis scale: 1 s/div.

power absorbed by the motor reactances. This is also evident from the phase difference of approximately 90° , between the phase-A voltage of VSI-2 (trace-c of Fig. 16) and the stator current in phase-A (trace-d, Fig. 16). As already explained, this phase difference will not be exactly 90° since VSI-2 draws a modest amount of active power to compensate for power losses at the inverter and capacitor. VSI-2 is actually injecting a series voltage for reactive power compensation which, in effect, also counters the increased reactive voltage drop in the motor reactance at high speeds.

The motor speed, modulation index of VSI-2, DC-link voltage of VSI-2 (capacitor voltage), and stator phase-A current during startup and acceleration of the FPIM- drive up to 1400 RPM are shown in Fig. 17. The capacitor voltage controller can maintain the capacitor voltage at the reference value during the changes in speed as shown in trace-c of Fig. 17. Since the DC-link voltage is fixed, the modulation index of VSI-2 (Fig. 17, trace-b) increases with increase in speed indicating the increase in reactive power delivered by VSI-2.

The motor speed, fundamental component of phase-A voltage generated by VSI-2 and the stator current in phase-A during the acceleration of the drive from 1000 RPM to 1900 RPM, 4.75 times the base speed of 400 RPM, and

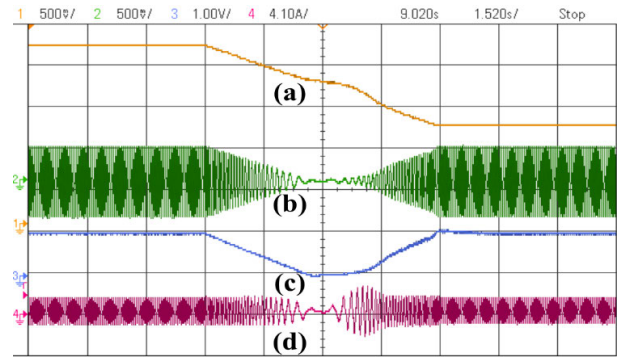


FIGURE 20. Experimental result: Speed reversal from 500 RPM to -500 RPM. a) Speed (500 RPM/div.) b) Fundamental component of phase-A voltage of VSI-2 (30 V/div.) c) Modulation index of VSI-2 (0.84/div.) d) Stator phase-A current (4.1 A/div.). X-axis scale: 1.52 s/div.

at 1.5 Nm load are shown in in Fig. 18. It is evident from this figure that the voltage generated by VSI-2 is increasing so as to deliver the increasing reactive power requirement of the motor as the speed increases.

The motor speed, modulation index of VSI-2, fundamental component of phase-A voltage generated by VSI-2, and the stator phase-A during acceleration are shown in Fig. 19. It is clear from Fig. 19 that the modulation index and consequently the voltage generated by VSI-2 are increasing to deliver the reactive power requirement by the drive as the speed increases beyond several times the base speed.

The waveforms corresponding to the speed reversal from 500 RPM to -500 RPM are shown in Fig. 20. The variation of the modulation index and hence the VSI-2 voltage during deceleration and acceleration in the reverse direction is clearly visible in this figure.

Though the experimental results are provided for closed loop V/f control, the proposed scheme can be very well incorporated in other high- performance control schemes like the field oriented control. The constant V/f control method is used for implementing the proposed scheme in order to focus and emphasize more on the main control strategy based on stator current vector oriented synchronous reference frame and the decoupled control of individual inverters, without going into the complexities of vector control. Both constant V/f ratio control method and the vector control method provide a voltage reference. The proposed scheme can accept voltage reference generated by any motor control algorithm.

VI. CONCLUSION

A new voltage space vector based control scheme for extending the speed range of dual inverter fed five phase induction motor drives with open-end stator windings is proposed in this article. In the proposed scheme, the voltage across the motor windings is realized by combining the orthogonal virtual voltage vectors generated by a DC source fed voltage source inverter (VSI) and a capacitor fed VSI. The virtual voltage vectors are generated in a decoupled manner so as to ensure that the DC source fed VSI supplies only active power to the drive thereby forcing the capacitor fed VSI

to supply the reactive power requirement of the system in the entire speed range. The magnitude of the virtual voltage vector generated by the capacitor fed VSI, which maintains a nearly quadrature relationship with the motor current space vector, is controlled to inject adequate voltage to overcome the increasing voltage drop across the motor reactances as the speed increases, while compensating the total reactive power requirement of the drive thereby facilitating the increase in the constant power speed range of the drive. The voltage references for the two VSIs are obtained by transforming the motor voltages to a synchronously revolving dq-stator reference frame wherein the d -axis is aligned with the motor current space vector. While generating the virtual voltage vectors of both inverters it is made sure that the average voltage generated in the auxiliary plane is nullified in a switching period thereby preventing circulation of large harmonic currents. The proposed scheme is substantially simpler compared to the existing schemes since it contains the least number of PI controllers. The proposed scheme is experimentally verified on a laboratory prototype under transient and steady state operating conditions covering the extended speed range up to 4.75 times the base speed. The experimental results confirm the potential of the proposed scheme to be considered for multiphase drive applications that require operation over a wide speed range with constrained DC source voltage.

REFERENCES

- [1] E. Levi, "Multiphase electric machines for variable-speed applications," *IEEE Trans. Ind. Electron.*, vol. 55, no. 5, pp. 1893–1909, May 2008.
- [2] I. Subotic, N. Bodo, and E. Levi, "Single-phase on-board integrated battery chargers for EVs based on multiphase machines," *IEEE Trans. Power Electron.*, vol. 31, no. 9, pp. 6511–6523, Sep. 2016.
- [3] C. A. Reusser, H. A. Young, J. R. P. Osses, M. A. Perez, and O. J. Simmonds, "Power electronics and drives: Applications to modern ship propulsion systems," *IEEE Ind. Electron. Mag.*, vol. 14, no. 4, pp. 106–122, Dec. 2020.
- [4] B. P. Reddy and S. Keerthipati, "Multilayer fractional slot pole-phase modulated induction motor drives for traction applications," *IEEE Trans. Ind. Electron.*, vol. 67, no. 11, pp. 9112–9119, Nov. 2020.
- [5] M. Mengoni, L. Zarri, A. Tani, L. Parsa, G. Serra, and D. Casadei, "High-torque-density control of multiphase induction motor drives operating over a wide speed range," *IEEE Trans. Ind. Electron.*, vol. 62, no. 2, pp. 814–825, Feb. 2015.
- [6] B. Wang, J. Zhang, Y. Yu, X. Zhang, and D. Xu, "Unified complex vector field-weakening control for induction motor high-speed drives," *IEEE Trans. Power Electron.*, vol. 36, no. 6, pp. 7000–7011, Jun. 2021.
- [7] S.-H. Kim and S.-K. Sul, "Voltage control strategy for maximum torque operation of an induction machine in the field-weakening region," *IEEE Trans. Ind. Electron.*, vol. 44, no. 4, pp. 512–518, Aug. 1997.
- [8] M. Mengoni, A. Amerise, L. Zarri, A. Tani, G. Serra, and D. Casadei, "Control scheme for open-ended induction motor drives with a floating capacitor bridge over a wide speed range," *IEEE Trans. Ind. Appl.*, vol. 53, no. 5, pp. 4504–4514, Sep. 2017.
- [9] I. J. Smith and J. Salmon, "High-efficiency operation of an open-ended winding induction motor using constant power factor control," *IEEE Trans. Power Electron.*, vol. 33, no. 12, pp. 10663–10672, Dec. 2018.
- [10] A. Amerise, M. Mengoni, L. Zarri, A. Tani, S. Rubino, and R. Bojoi, "Open-end windings induction motor drive with floating capacitor bridge at variable DC-link voltage," *IEEE Trans. Ind. Appl.*, vol. 55, no. 3, pp. 2741–2749, May 2019.
- [11] L. Mohan, K. Pant, and P. P. Rajeevan, "A speed range extension scheme for scalar-controlled open-end winding induction motor drives," *IEEE Trans. Ind. Appl.*, vol. 58, no. 2, pp. 2055–2062, Mar. 2022.
- [12] X. Sun, Z. Liu, D. Jiang, and W. Kong, "Control of five-phase open-end induction machine drive topology with floating capacitors at optimized DC voltage," in *Proc. IEEE Energy Convers. Congr. Expo. (ECCE)*, Baltimore, MD, USA, Sep. 2019, pp. 7072–7077.
- [13] X. Sun, Z. Liu, D. Jiang, and W. Kong, "Multiphase open-end winding induction machine drive with the floating capacitor," *IEEE Trans. Ind. Appl.*, vol. 56, no. 5, pp. 5013–5022, Sep. 2020.
- [14] H. Wang, P. Davari, H. Wang, D. Kumar, F. Zare, and F. Blaabjerg, "Lifetime estimation of DC-link capacitors in adjustable speed drives under grid voltage unbalances," *IEEE Trans. Power Electron.*, vol. 34, no. 5, pp. 4064–4078, May 2019.
- [15] Z. Liu, Z. Zheng, L. Xu, K. Wang, and Y. Li, "Current balance control for symmetrical multiphase inverters," *IEEE Trans. Power Electron.*, vol. 31, no. 6, pp. 4005–4012, Jun. 2016.
- [16] P. S. N. de Silva, J. E. Fletcher, and B. W. Williams, "Development of space vector modulation strategies for five phase voltage source inverters," in *Proc. 2nd IEE Int. Conf. Power Electron., Mach. Drives*, Mar. 2004, pp. 650–655.
- [17] A. Iqbal and E. Levi, "Space vector modulation schemes for a five-phase voltage source inverter," in *Proc. Eur. Conf. Power Electron. Appl.*, Dresden, Germany, Sep. 2005, p. 12.



PRASOON CHANDRAN MAVILA (Member, IEEE) received the B.Tech. degree in electrical and electronics engineering from the Cochin University of Science and Technology (CUSAT), Kerala, India, in 2014, and the M.Tech. degree in power electronics and drives from the Government Engineering College Kannur, Kerala, in 2016. He is currently pursuing the Ph.D. degree with the Department of Avionics, Indian Institute of Space Science and Technology, Thiruvananthapuram, India. His research interests include the control of multiphase electrical drives, power converters, and PWM techniques.



P. P. RAJEEVAN (Senior Member, IEEE) received the Ph.D. degree in power electronics from the Indian Institute of Science, Bengaluru, India. He is currently a Professor with the Department of Avionics, Indian Institute of Space Science and Technology, Thiruvananthapuram, India. His research interests include the control of electric drives, power electronic converters, pulse width modulation techniques, renewable energy, and power quality.

...